Devil's staircase continuum in the chiral clock spin glass with competing ferromagnetic-antiferromagnetic and left-right chiral interactions

Tolga Çağlar[1] and A. Nihat Berker[1,2,3]

[1]*Faculty of Engineering and Natural Sciences, Sabancı University, Tuzla, Istanbul 34956, Turkey*

[2]*Faculty of Engineering and Natural Sciences, Kadir Has University, Cibali, Istanbul 34083, Turkey*

[3]*Department of Physics, Massachusetts Institute of Technology, Cambridge, Massachusetts 02139, USA*

The chiral clock spin-glass model with $q = 5$ states, with both competing ferromagnetic-antiferromagnetic and left-right chiral frustrations, is studied in $d = 3$ spatial dimensions by renormalization-group theory. The global phase diagram is calculated in temperature, antiferromagnetic bond concentration p, random chirality strength, and right-chirality concentration c. The system has a ferromagnetic phase, a multitude of different chiral phases, a chiral spin-glass phase, and a critical (algebraically) ordered phase. The ferromagnetic and chiral phases accumulate at the disordered phase boundary and form a spectrum of devil's staircases, where different ordered phases characteristically intercede at all scales of phase-diagram space. Shallow and deep reentrances of the disordered phase, bordered by fragments of regular and temperature-inverted devil's staircases, are seen. The extremely rich phase diagrams are presented as continuously and qualitatively changing videos.

I. INTRODUCTION

The presence of chiral interactions, motivated by experimental systems [1–5], can result in extremely rich phase transition phenomena in otherwise simple systems [6]. In this respect, we study here a $q = 5$ state clock spin-glass model in $d = 3$ spatial dimensions, using renormalization-group theory. Our system has both competing ferromagnetic and antiferromagnetic interactions, as in the usually studied spin-glass models [8], and competing left-chiral and right-chiral interactions [6]. We have studied $q = 5$ states, because odd numbers of states have built-in entropy for antiferromagnetic interactions, even without quenched randomness and frustration [7].

The global phase diagram is calculated in temperature, antiferromagnetic bond concentration p, random chirality strength, and right-chirality concentration c. We find an extremely rich phase diagram, with a ferromagnetic phase, a multitude of different chiral phases, a chiral spin-glass phase, and a critical (algebraically) ordered phase [9,10]. The ferromagnetic and chiral phases accumulate at the disordered phase boundary and form devil's staircases [11,12], where different ordered phases characteristically intercede at all scales of phase-diagram space. In fact, a continuum of devil's staircases is found. Shallow and deep reentrances of the disordered phase, bordered by fragments of regular and temperature-inverted devil's staircases, are seen. The extremely rich phase diagrams are presented as continuously and qualitatively changing videos [13].

II. THE q-STATE CHIRAL CLOCK DOUBLE SPIN GLASS

The q-state clock spin glass is composed of unit spins that are confined to a plane and that can only point along q angularly equidistant directions, with Hamiltonian

$$-\beta\mathcal{H} = \sum_{\langle ij \rangle} J_{ij}\vec{s}_i \cdot \vec{s}_j = \sum_{\langle ij \rangle} J_{ij}\cos\theta_{ij}, \qquad (1)$$

where $\beta = 1/k_B T$, $\theta_{ij} = \theta_i - \theta_j$, at each site i the spin angle θ_i takes on the values $(2\pi/q)\sigma_i$ with $\sigma_i = 0,1,2,\ldots,(q-1)$, and $\langle ij \rangle$ denotes that the sum runs over all nearest-neighbor pairs of sites. As a ferromagnetic-antiferromagnetic spin-glass system [8], the bond strengths J_{ij}, with quenched (frozen) ferromagnetic-antiferromagnetic randomness, are $+J > 0$ (ferromagnetic) with probability $1 - p$ and $-J$ (antiferromagnetic) with probability p, with $0 \leqslant p \leqslant 1$. Thus, the ferromagnetic and antiferromagnetic interactions locally compete in frustration centers. Recent studies on ferromagnetic-antiferromagnetic clock spin glasses are in Refs. [7,14,15].

In the q-state chiral clock double spin glass introduced here, frustration also occurs via randomly frozen left or right chirality [6]. The Hamiltonian in Eq. (1) is generalized to random local chirality,

$$-\beta\mathcal{H} = \sum_{\langle ij \rangle} \left[J_{ij}\cos\theta_{ij} + \Delta\,\delta\left(\theta_{ij} + \eta_{ij}\frac{2\pi}{q}\right) \right]. \qquad (2)$$

In a cubic lattice, the $x, y,$ or z coordinates increase as sites along the respective coordinate direction are considered. Bond moving as in Fig. 1(a) is done transversely to the bond directions, so that this sequencing is respected. Equivalently, in the corresponding hierarchical lattice, one can always define a direction along the connectivity, for example, from left to right in Fig. 1(b), and assign consecutive increasing number labels to the sites. In Eq. (2), for each pair of nearest-neighbor sites $\langle ij \rangle$ the numerical site label j is ahead of i, frozen (quenched) $\eta_{ij} = 1$ (left chirality) or -1 (right chirality), and the δ function $\delta(x) = 1\,(0)$ for $x = 0\,(x \neq 0)$. The overall concentrations of left and right chirality are respectively $1 - c$ and c, with $0 \leqslant c \leqslant 1$. The strength of the random chiral interaction is Δ/J, with temperature divided out. With no loss of generality, we take $\Delta \geqslant 0$. Thus, the system is chiral for $\Delta > 0$, chiral symmetric for $c = 0.5$, and chiral symmetry broken for $c \neq 0.5$. The global phase diagram is in terms of temperature J^{-1}, antiferromagnetic bond concentration p, random chirality strength Δ/J, and chiral symmetry-breaking concentration c.
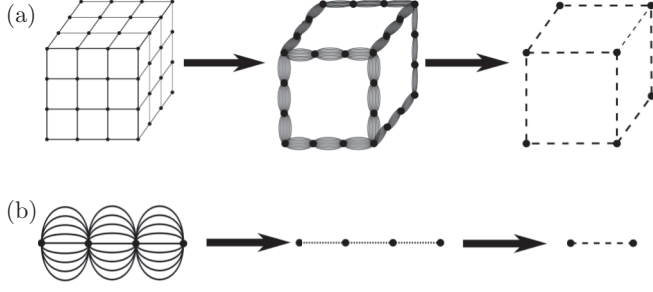
FIG. 1. (a) The Migdal-Kadanoff approximate renormalization-group transformation for the cubic lattice, composed of the bond-moving followed by decimation steps, with the length rescaling factor $b = 3$. The corresponding hierarchical lattice is obtained by the repeated self-imbedding of the leftmost graph in panel (b). (b) The exact renormalization-group transformation for this $d = 3$ hierarchical lattice. The two procedures yield identical recursion relations.

III. RENORMALIZATION-GROUP METHOD: MIGDAL-KADANOFF APPROXIMATION AND EXACT HIERARCHICAL LATTICE SOLUTION

We solve the chiral clock double spin-glass model with $q = 5$ states by renormalization-group theory, in $d = 3$ spatial dimensions, with length rescaling factor $b = 3$. We use $b = 3$, as in previous position-space renormalization-group calculations of spin-glass systems, because it treats ferromagnetism and antiferromagnetism on equal footing. Our solution is, simultaneously, the Migdal-Kadanoff approximation [16,17] for the cubic lattice and the exact solution [18–22] for the $d = 3$ hierarchical lattice based on the repeated self-imbedding of leftmost graph of Fig. 1(b). Figure 1(a) shows the Migdal-Kadanoff approximate renormalization-group transformation for the cubic lattice, composed of the bond-moving followed by decimation steps. Figure 1(b) shows the exact renormalization-group transformation for the hierarchical lattice. The two procedures yield identical recursion relations.

Exact calculations on hierarchical lattices are also currently widely used on a variety of statistical mechanics problems [23–39]. On the other hand, this approximation for the cubic lattice is an uncontrolled approximation, as in fact are all renormalization-group theory calculations in $d = 3$ and all mean-field theory calculations. However, as noted before [40], the local summation in position-space technique used here has been qualitatively, near quantitatively, and predictively successful in a large variety of problems, such as arbitrary spin-s Ising models [41], global Blume-Emery-Griffiths model [42], first- and second-order Potts transitions [43,44], antiferromagnetic Potts critical phases [9,10], ordering [45] and superfluidity [46] on surfaces, multiply re-entrant liquid crystal phases [47,48], chaotic spin glasses [49], random-field [50,51] and random-temperature [52,53] magnets including the remarkably small $d = 3$ magnetization critical exponent β of the random-field Ising model, and high-temperature superconductors [54].

Under the renormalization-group transformation described below, the Hamiltonian of Eq. (2) maps onto the more general form

$$-\beta\mathcal{H} = \sum_{\langle ij \rangle} V_{ij}(\theta_{ij}), \qquad (3)$$

where $\theta_{ij} = \theta_i - \theta_j$ can take q different values, so that for each pair $\langle ij \rangle$ of nearest-neighbor sites, there are q different interaction constants

$$\{V_{ij}(\theta_{ij})\} = \{V_{ij}(0), V_{ij}(\delta), V_{ij}(2\delta), V_{ij}(3\delta), V_{ij}(4\delta)\} \equiv \mathbf{V}_{ij}, \quad (4)$$

which are in general different at each locality (quenched randomness). Here, $\delta \equiv 2\pi/5$ is the angle between consecutive clock-spin directions. The largest element of $\{V_{ij}(\theta_{ij})\}$ at each locality $\langle ij \rangle$ is set to zero, by subtracting the same constant G from all q interaction constants, with no effect on the physics; thus, the $q - 1$ other interaction constants are negative.

The local renormalization-group transformation is achieved by the sequence, shown in Fig. 1, of bond movings

$$\widetilde{V}_{ij}(\theta_{ij}) - \widetilde{G} = \sum_{k=1}^{b^{d-1}} V_{ij}^{(k)}(\theta_{ij}), \qquad (5)$$

and decimations

$$e^{V'_{14}(\theta_{14}) - G} = \sum_{\theta_2, \theta_3} e^{\widetilde{V}_{12}(\theta_{12}) + \widetilde{V}_{23}(\theta_{23}) + \widetilde{V}_{34}(\theta_{34})}, \qquad (6)$$

where $\widetilde{G}$ and G are the subtractive constants mentioned above, and prime marks the interaction of the renormalized system.

The starting double-bimodal quenched probability distribution of the interactions, characterized by p and c as described above, is not conserved under rescaling. The renormalized quenched probability distribution of the interactions is obtained by the convolution [55]

$$P'(\mathbf{V}'_{i'j'}) = \int \left\{ \prod_{ij}^{i'j'} d\mathbf{V}_{ij} P(\mathbf{V}_{ij}) \right\} \delta(\mathbf{V}'_{i'j'} - \mathbf{R}(\{\mathbf{V}_{ij}\})), \quad (7)$$

where $\mathbf{V}_{ij} \equiv \{V_{ij}(\theta_{ij})\}$ as in Eq. (4), $\mathbf{R}(\{\mathbf{V}_{ij}\})$ represents the bond moving and bond decimation given in Eqs. (5) and (6), and primes refer to the renormalized system. Similar previous studies, on other spin-glass systems, are in Refs. [7,14,56–63]. For numerical practicality, the bond moving and decimation of Eqs. (5) and (6) are achieved by a sequential pairwise combination of interactions, each pairwise combination leading to an intermediate probability distribution resulting from a pairwise convolution as in Eq. (7).

We effect this procedure numerically, first starting with the initial double δ distribution of Eq. (2), giving 4 possible interactions quenched randomly distributed throughout the system, and generating 1000 interactions that embody the quenched probability distribution resulting from the pairwise combination. Each of the generated 1000 interactions is described by q interaction constants, as explained above [Eq. (4)]. At each subsequent pairwise convolution as in Eq. (7), 1000 randomly chosen pairs, representing quenched random neighbors in the lattice, are matched by (5) or (6), and a new set of 1000 interactions is produced. As a control, we have also calculated phase diagrams given below using 1500 interactions and the phase diagrams did not change.

Our calculation simply consists in following the recursion relations, Eqs. (5)–(7), to the various fixed points and thereby
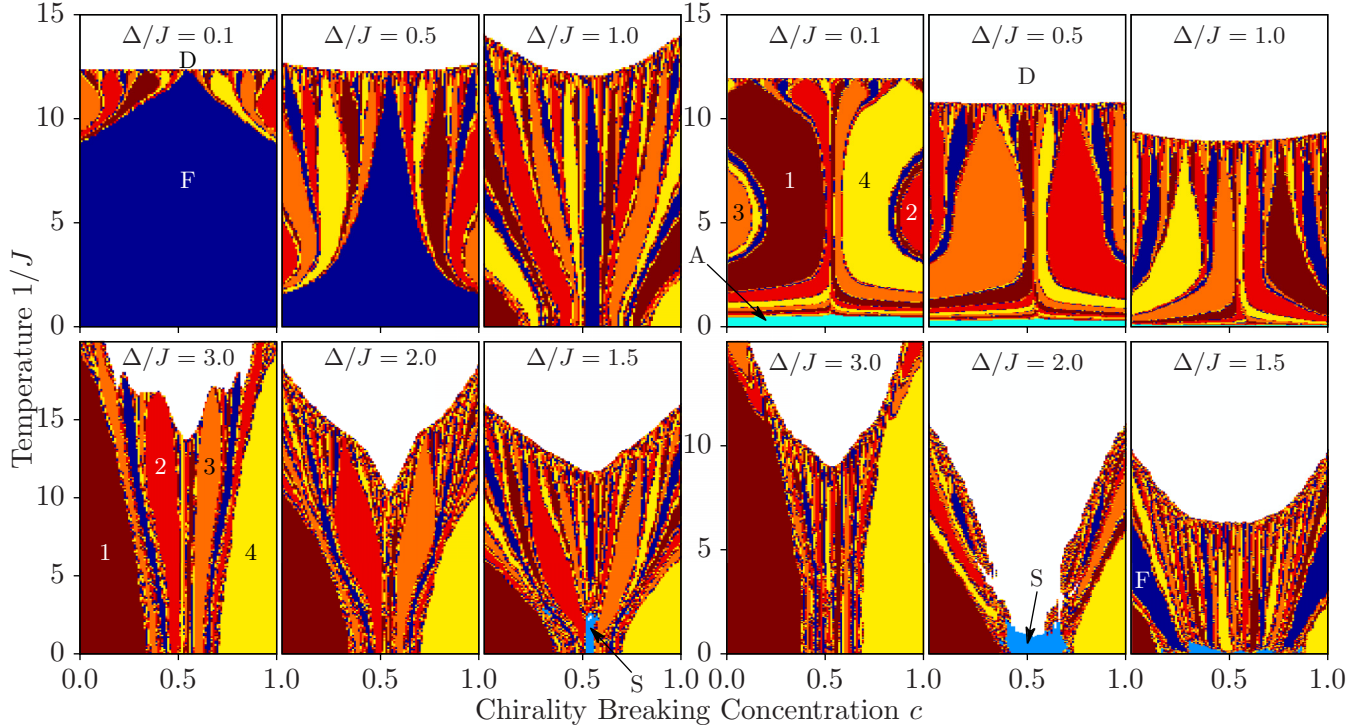
FIG. 2. Calculated sequence of phase diagrams for the ferromagnetic ($p = 0$), on the left side of the figure, and antiferromagnetic ($p = 1$), on the right side, systems with quenched random left- and right-chiral interactions. The horizontal axis c is the concentration of right-chiral interactions. Phase diagrams for different random chirality strengths Δ/J are shown. The system exhibits ferromagnetic (F), a multitude of different chiral, and spin-glass (S) ordered phases. On some of the chiral phases, the δ multiplicity of the asymptotically dominant interaction is indicated. The ferromagnetic and chiral phases accumulate as different devil's staircases at their boundary with the disordered (D) phase. The antiferromagnetic system also exhibits an algebraically ordered (A) phase. The full richness of the continuum of widely varying devil's staircase phase diagrams can also be seen in video form, four of which are accessible as Supplemental Material [13].

mapping the initial conditions that are the basins of attraction of the various fixed points. This map is the phase diagram: The different thermodynamic phases of the system are identified by the different asymptotic renormalization-group flows of the quenched probability distribution $P(\mathbf{V}_{ij})$. Two renormalization-group trajectories starting at each side of a phase boundary point diverge from each other, flowing towards the phase sinks (completely stable fixed points) of their respective phases. Thus, the phase boundary point between two phases is readily obtained to the accuracy of the figures. We are therefore able to calculate the global phase diagram of the chiral clock double spin-glass model.

IV. GLOBAL PHASE DIAGRAM OF THE $q = 5$ STATE CHIRAL CLOCK DOUBLE SPIN GLASS

The global phase diagram of the $q = 5$ state chiral clock double spin-glass model in $d = 3$ spatial dimensions, in temperature J^{-1}, antiferromagnetic bond concentration p, random chirality strength Δ/J, and right-chirality concentration c, is a four-dimensional object, so that only the cross sections of the global phase diagram are exhibited.

Figure 2 shows the calculated sequence of phase diagrams for the ferromagnetic ($p = 0$), on the left side of the figure, and antiferromagnetic ($p = 1$), on the right side, systems with quenched random left- and right-chiral interactions. The horizontal axis c is the concentration of right-chiral interactions.

Phase diagrams for different random chirality strengths Δ/J are shown. The system exhibits ferromagnetic (F), a multitude of different chiral, and spin-glass (S) ordered phases. The antiferromagnetic system also shows an algebraically (A) ordered (critical) phase, in which every point is a critical point with divergent correlation length [9,10]. In all cases, the ferromagnetic and different chiral phases accumulate as different devil's staircases [11,12] at their boundary with the disordered (D) phase. The definition of the devil's staircase is that this accumulation is seen at every expanded scale of the phase diagram variables. This accumulation at every expanded phase diagram scale is indeed revealed from our calculations, as seen further below.

Figure 3 shows the calculated sequence of phase diagrams for the left chiral ($c = 0$), on the upper side, and quenched random left and right chiral ($c = 0.5$), on the lower side, system with, in both cases, quenched random ferromagnetic and antiferromagnetic interactions. The horizontal axis is the random chirality strength Δ/J. The consecutive phase diagrams are for different concentrations of antiferromagnetic interactions p. The system exhibits ferromagnetic (F), a multitude of different chiral, spin-glass (S), and algebraically ordered (A) phases. The ferromagnetic and different chiral phases accumulate as different devil's staircases [11,12] at their boundary with the disordered (D) phase. Note shallow and deep re-entrances of disorder [48,64–67] at $p = 0.4$ and $p = 0.7$, respectively, surrounded by regular and temperature-inverted devil's staircases.
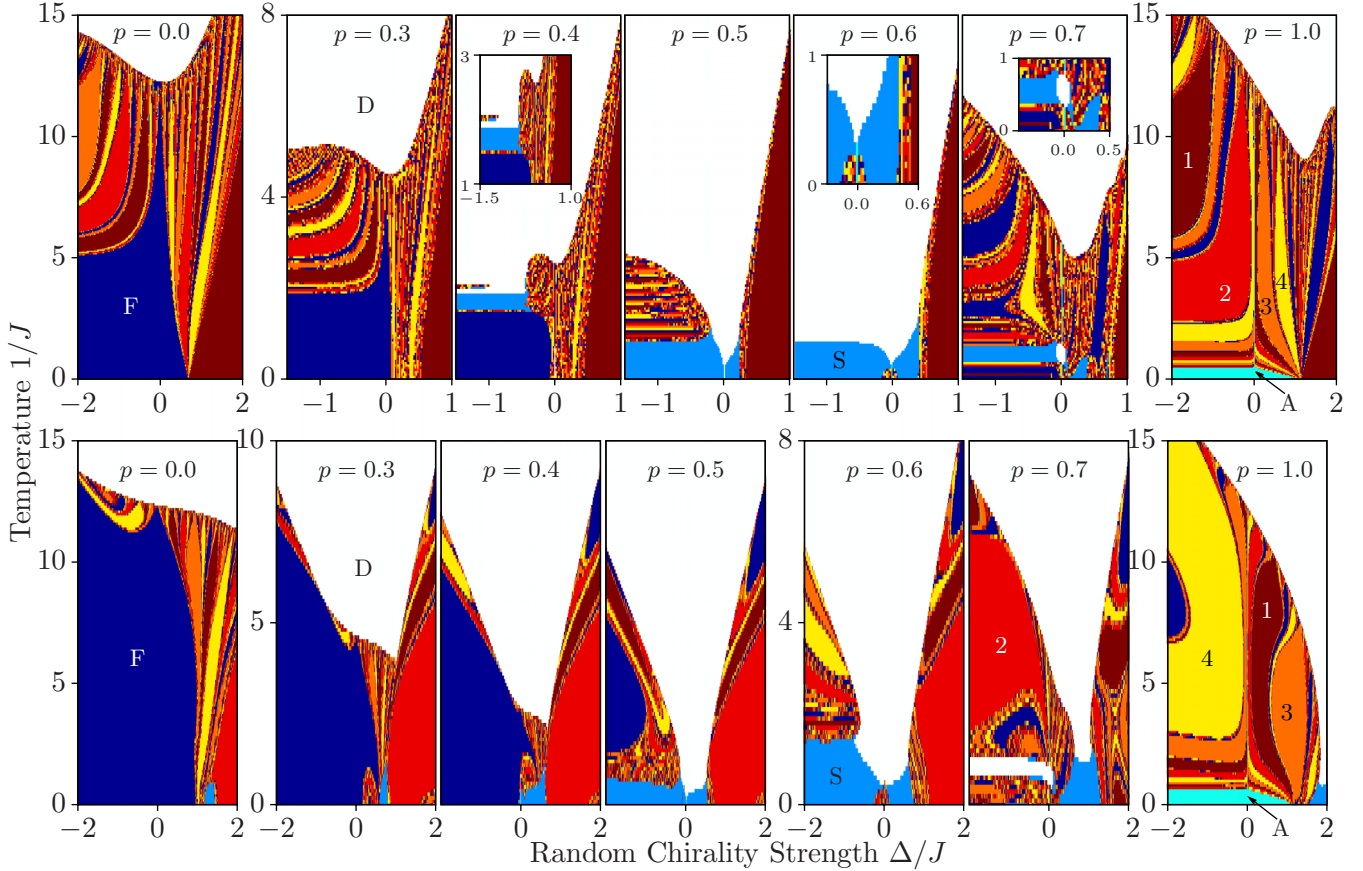
FIG. 3. Calculated sequence of phase diagrams for the left-chiral ($c = 0$), on the upper side of the figure, and quenched random left- and right-chiral ($c = 0.5$), on the lower side, systems with quenched random ferromagnetic and antiferromagnetic interactions. The horizontal axis is the random chirality strength Δ/J. The consecutive phase diagrams are for different concentrations of antiferromagnetic interactions p. The system exhibits ferromagnetic (F), a multitude of different chiral, spin-glass (S), and critical (algebraically) ordered (A) phases. On some of the chiral phases, the δ multiplicity of the asymptotically dominant interaction is indicated. The ferromagnetic and chiral phases accumulate as different devil's staircases at their boundary with the disordered (D) phase. Note shallow and deep reentrances of the disordered phase at $p = 0.4$ and $p = 0.7$, respectively, surrounded by regular and temperature-inverted devil's staircases. The full richness of the continuum of widely varying devil's staircase phase diagrams can also be seen in video form, four of which are accessible as Supplemental Material [13].

Figure 4 shows the phase diagram cross section in the upper left of Fig. 3, with calculated 10-fold and 100-fold zoom. The devil's staircase structure appears at each zoom level.

The full richness of the continuum of widely varying devil's staircase phase diagrams can best be seen in video form, four of which are accessible as Supplemental Material [13]. These videos effectively exhibit a very large number of calculated phase diagram cross sections.

V. ENTIRE-PHASE CRITICALITY, DIFFERENTIATED CHAOS IN THE SPIN-GLASS AND AT ITS BOUNDARY

The renormalization-group mechanism for the algebraically ordered (critical) phase is that all renormalization-group trajectories originating inside this phase flow to a completely stable fixed point (sink) that occurs at finite temperature (finite coupling strength) [9,10,68–76]. In all other ordered phases, the trajectories flow to strong (infinite) coupling.

In the ferromagnetic phase, the interaction $V_{ij}(0)$ becomes asymptotically dominant. In the chiral phases, in the renormalization-group trajectories, one of the chiral interactions from the right-hand side of Eq. (4),

$\{V_{ij}(\delta), V_{ij}(2\delta), V_{ij}(3\delta), V_{ij}(4\delta)\}$, becomes asymptotically dominant. However, in each of the separate phases, it takes a characteristic number n of renormalization-group transformations, namely a length scale of 3^n, to reach the dominance of one chiral interaction. This distinct number of iterations, namely scale changes, determines, by tracing back to the periodic sequence in the original lattice, the pitch of the chiral phase in the original unrenormalized system. Thus, the chiral phases in the original unrenormalized system, with distinct chiral pitches, are distinct phases. After the dominance of one chiral interaction, the renormalization-group trajectory follows the periodic sequence $V_{ij}(\delta) \rightarrow V_{ij}(3\delta) \rightarrow V_{ij}(4\delta) \rightarrow V_{ij}(2\delta) \rightarrow V_{ij}(\delta)$ resulting from matching $q = 5$ and $b = 3$.

Our calculation is exact for the hierarchical lattice pictured in Fig. 1(b); therefore the phase diagrams in Figs. 2 and 3 are exactly applicable. However, our calculation is approximate for the cubic lattice, as pictured in Fig. 1(a). Thus, one could speculate that in the cubic lattice, the multitude of chiral phases would appear as a single chiral phase with a continuously varying pitch: Figure 5 shows all the chiral phases merged into a single phase. It is seen that a quite unusual phase diagram
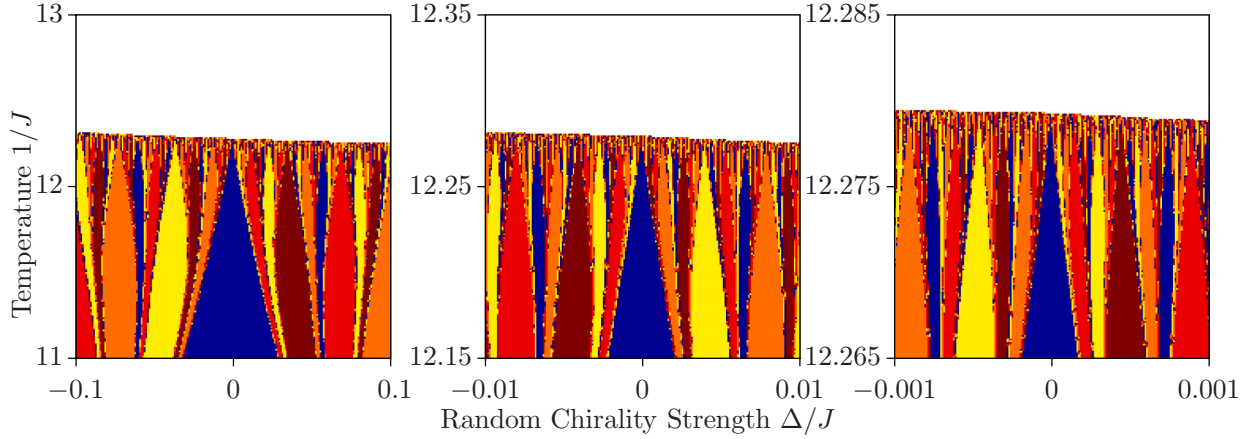
FIG. 4. The phase diagram cross section in the upper left of Fig. 3, with a calculated 10-fold zoom and 100-fold zoom. The devil's staircase structure appears at each zoom level.

still appears, with the interlacing of the ferromagnetic phase with the chiral phase, throughout the bulk of the phase region.

The renormalization-group trajectories starting in the chiral spin-glass phase, unlike those in the ferromagnetic or chiral phases, do not have the asymptotic behavior where at any scale a single potential $V(\theta)$ is dominant. These trajectories of the spin-glass phase asymptotically go to a strong-coupling fixed probability distribution $P(\mathbf{V}_{ij})$ which assigns nonzero probabilities to a distribution of $\mathbf{V}_{ij}$ values, with no single $V_{ij}(\theta)$ being dominant. Projections of this distribution (a

function of five variables) are shown in Fig. 6. This situation is a direct generalization of the asymptotic trajectories of the $\pm J$ Ising spin-glass phase, where a fixed probability distribution over positive and negative values of the interaction J is obtained, with no single value of J being dominant [14].

Since, at each locality, the largest interaction in $\{V_{ij}(0), V_{ij}(\delta), V_{ij}(2\delta), V_{ij}(3\delta), V_{ij}(4\delta)\}$ is set to zero and the four other interactions are thus made negative, by subtracting the same constant from all five interactions without affecting the physics, the quenched probability distribution $P(\mathbf{V}_{ij})$,
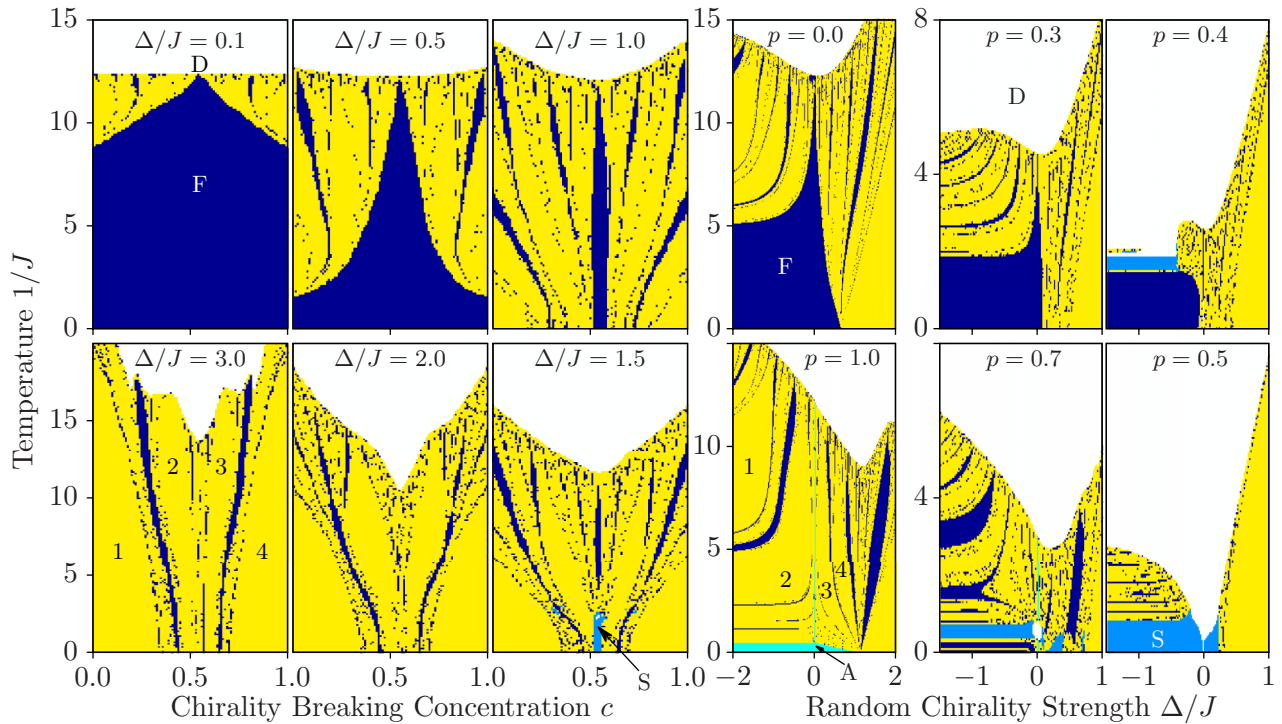

FIG. 5. Our calculation is exact for the hierarchical lattice pictured in Fig. 1(b); therefore the phase diagrams in Figs. 2 and 3 are exactly applicable. However, our calculation is approximate for the cubic lattice, as pictured in Fig. 1(a). Thus, it could be speculated that in the cubic lattice, the multitude of chiral phases would appear as a single chiral phase with a continuously varying pitch: This figure shows all the chiral phases merged into a single phase. It is seen that a quite unusual phase diagram still appears, with the interlacing of the ferromagnetic phase with the chiral phase, throughout the bulk of the phase region. The left side of this figure is derived from the left portion of Fig. 2; the right side is derived from the top portion of Fig. 3.
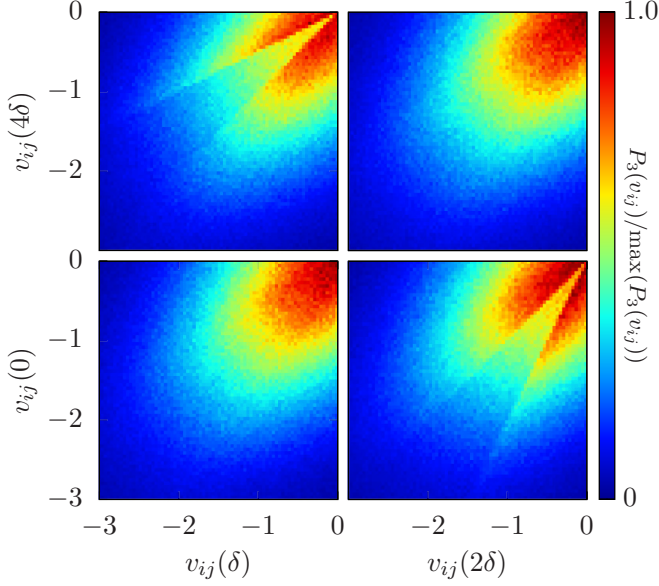
FIG. 6. Asymptotic fixed distribution of the spin-glass phase. The part of the fixed distribution, $P_3(\mathbf{V}_{ij})$ for the interactions $\mathbf{V}_{ij}$ in which $V_{ij}(3\delta)$ is maximum and therefore 0 (and the other four interactions are negative) is shown in this figure, with $v_{ij}(\sigma\delta) = V_{ij}(\sigma\delta)/\langle|V_{ij}(\sigma\delta)|\rangle$. The projections of $P_3(\mathbf{V}_{ij})$ onto two of its four arguments are shown in each panel of this figure. The other four $P_\sigma(\mathbf{V}_{ij})$ have the same fixed distribution. Thus, chirality is broken locally but not globally.

a function of five variables, is actually composed of five functions $P_\sigma(\mathbf{V}_{ij})$ of four variables, each such function corresponding to one of the interactions being zero and the other four, arguments of the function, being negative. Figure 6 shows one of the latter functions: The part of the fixed distribution, $P_3(\mathbf{V}_{ij})$, for the interactions $\mathbf{V}_{ij}$ in which $V_{ij}(3\delta)$ is maximum and therefore 0 (and the other four interactions are negative) is shown in this figure. The projections of $P_3(\mathbf{V}_{ij})$ onto two of its four arguments are shown in each panel of this figure. The other four $P_\sigma(\mathbf{V}_{ij})$ have the same fixed distribution. Thus, chirality is broken locally, but not globally.

Another distinctive mechanism, that of chaos under scale change [49,77,78] or, equivalently, under spatial translation [14], occurs within the spin-glass phase and differently at the spin-glass phase boundary [14], in systems with competing ferromagnetic and antiferromagnetic interactions [14,49,62,77–105] and, more recently, with competing left- and right-chiral interactions [6]. The physical hierarchical lattice that we solve here is an infinite system, where 1000 quintuplets $\{V_{ij}(0), V_{ij}(\delta), V_{ij}(2\delta), V_{ij}(3\delta), V_{ij}(4\delta)\}$ are randomly distributed over the lattice bond positions. Thus, as we can fix our attention to one lattice position and monitor how the quintuplet at that position evolves under renormalization-group transformation, as it merges with its neighbors through bond moving [Eq. (5)] and decimation [Eq. (6)], and thereby calculate the Lyapunov exponent [14,62], which when positive is the measure of the strength of chaos.

Figure 7 gives the asymptotic chaotic renormalization-group trajectories of the spin-glass phase and, distinctly, of the phase boundary between the spin-glass and disordered
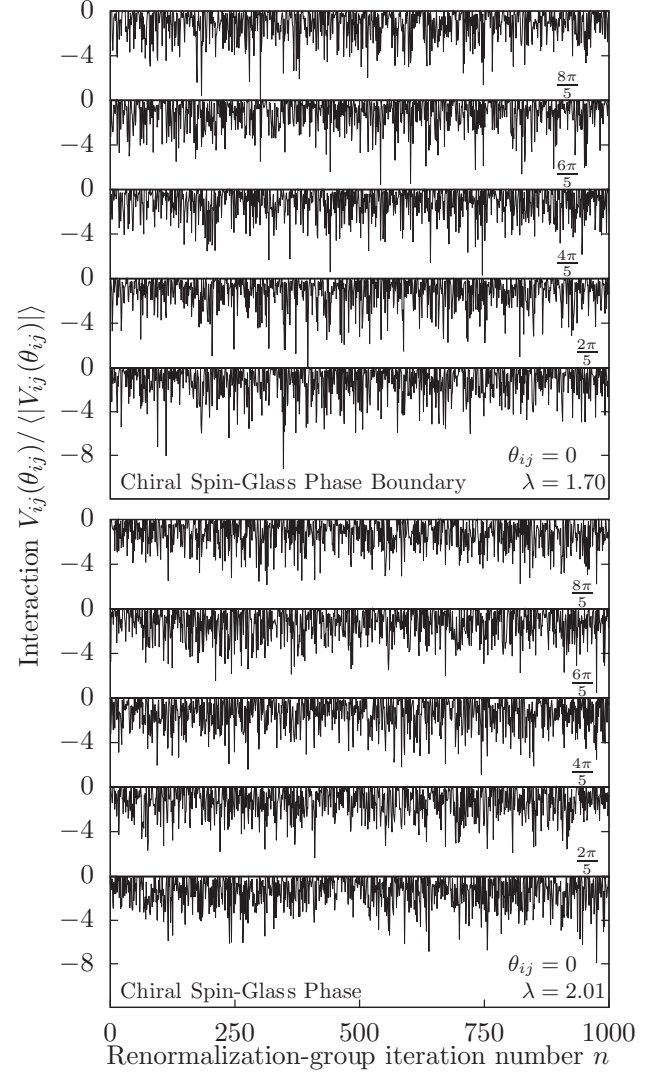

FIG. 7. Chaotic renormalization-group trajectories of the spin-glass phase (bottom) and of the phase boundary between the spin-glass and disordered phases (top). The five interactions $V_{ij}(0), V_{ij}(\delta), V_{ij}(2\delta), V_{ij}(3\delta), V_{ij}(4\delta)$ at a given location $\langle ij \rangle$, under consecutive renormalization-group transformations, are shown. The $\theta_{ij} = \sigma\delta$ angular value of each interaction $V_{ij}(\theta_{ij})$ is indicated in the figure panels. Bottom panel: Inside the spin-glass phase. The corresponding Lyapunov exponent is $\lambda = 2.01$ and the average interaction diverges as $\langle|V|\rangle \sim b^{y_R n}$, where n is the number of renormalization-group iterations and $y_R = 0.26$ is the runaway exponent. Top panel: At the phase boundary between the spin-glass and disordered phases. The corresponding Lyapunov exponent is $\lambda = 1.70$ and the average nonzero interaction remains fixed at $\langle V \rangle = -0.99$. As indicated by the Lyapunov exponents, chaos is stronger inside the spin-glass phase than at its phase boundary.

phases. The chaotic trajectories found here are similar to those found in traditional (Ising) spin-glasses [14,62], with of course different Lyapunov exponents seen below. The five interactions $V_{ij}(0), V_{ij}(\delta), V_{ij}(2\delta), V_{ij}(3\delta), V_{ij}(4\delta)$ at a given location $\langle ij \rangle$, under consecutive renormalization-group transformations, are shown in Fig. 7. As noted, chaos is measured by the Lyapunov exponent [14,62,96,106,107], which we here generalize, by

the matrix form, to our multiinteraction case:

$$\lambda = \lim_{n \to \infty} \frac{1}{n} \ln \left| \mathcal{E} \left(\prod_{k=0}^{n-1} \frac{d\mathbf{v}_{k+1}}{d\mathbf{v}_k} \right) \right|, \qquad (8)$$

where the function $\mathcal{E}(\mathbf{M})$ gives the largest eigenvalue of its matrix argument $\mathbf{M}$ and the vector $\mathbf{v}_k$ is

$$\mathbf{v}_k = \{ v_{ij}(0), v_{ij}(\delta), v_{ij}(2\delta), v_{ij}(3\delta), v_{ij}(4\delta) \}, \qquad (9)$$

with $v_{ij}(\sigma\delta) = V_{ij}(\sigma\delta)/\langle |V_{ij}(\sigma\delta)| \rangle$, at step k of the renormalization-group trajectory. The product in Eq. (8) is to be taken within the asymptotic chaotic band, which is renormalization-group stable or unstable for the spin-glass phase or its boundary, respectively. Thus, we throw out the first 100 renormalization-group iterations to eliminate the transient points outside of, but leading to, the chaotic band. Subsequently, typically using 1000 renormalization-group iterations in the product in Eq. (8) assures the convergence of the Lyapunov exponent value λ, which is thus accurate to the number of significant figures given. Spin-glass chaos occurs for $\lambda > 0$ [96] and as chaos is stronger, λ is more positive, as seen, for example, in the progressions in Figs. 6 and 7 of Ref. [62]. In the spin-glass phase of the currently studied system, the Lyapunov exponent is $\lambda = 2.01$ and the average interaction diverges as $\langle |V| \rangle \sim b^{y_R n}$, where n is the number of renormalization-group iterations and $y_R = 0.26$ is

the runaway exponent. At the phase boundary between the spin-glass and disordered phases, the Lyapunov exponent is $\lambda = 1.70$ and the average nonzero interaction remains fixed at $\langle V \rangle = -0.99$. As indicated by the Lyapunov exponents, chaos is stronger inside the spin-glass phase than at its phase boundary.

VI. CONCLUSION

It is thus seen that chirality and chiral quenched randomness provides, in a simple model, remarkably rich phase transition phenomena. These include a multitude of chiral phases, a continuum of widely varying devil's staircases, shallow and deep re-entrances of the disordered phase surrounded by regular and temperature-inverted devil's staircases, a critical phase, and a chiral spin-glass phase with chaotic rescaling behavior inside and differently at its boundary. The widely varying continuum of devil's staircase phase diagrams are best seen in video form, four of which are accessible as Supplemental Material [13]. Finally, the study of an even number of q states, which do not have a built-in entropy as mentioned above, should yield equally rich but qualitatively different phase diagrams.

[1] S. Ostlund, Phys. Rev. B **24**, 398 (1981).

[2] M. Kardar and A. N. Berker, Phys. Rev. Lett. **48**, 1552 (1982).

[3] D. A. Huse and M. E. Fisher, Phys. Rev. Lett. **49**, 793 (1982).

[4] D. A. Huse and M. E. Fisher, Phys. Rev. B **29**, 239 (1984).

[5] R. G. Caflisch, A. N. Berker, and M. Kardar, Phys. Rev. B **31**, 4527 (1985).

[6] T. Çağlar and A. N. Berker, Phys. Rev. E **94**, 032121 (2016).

[7] E. Ilker and A. N. Berker, Phys. Rev. E **90**, 062112 (2014).

[8] H. Nishimori, *Statistical Physics of Spin Glasses and Information Processing* (Oxford University Press, Oxford, UK, 2001).

[9] A. N. Berker and L. P. Kadanoff, J. Phys. A **13**, L259 (1980).

[10] A. N. Berker and L. P. Kadanoff, J. Phys. A **13**, 3786 (1980).

[11] P. Bak and R. Bruinsma, Phys. Rev. Lett. **49**, 249 (1982).

[12] A. Fukuda, Y. Takanishi, T. Isozaki, K. Ishikawa, and H. Takezoe, J. Mat. Chem. **4**, 997 (1994).

[13] See Supplemental Material at http://link.aps.org/supplemental/10.1103/PhysRevE.95.042125 for extremely rich devil's staircase phase diagrams presented as four continuously and qualitatively changing videos.

[14] E. Ilker and A. N. Berker, Phys. Rev. E **87**, 032124 (2013).

[15] C. Lupo and F. Ricci-Tersenghi, Phys. Rev. B **95**, 054433 (2017).

[16] A. A. Migdal, Zh. Eksp. Teor. Fiz. **69**, 1457 (1975) [Sov. Phys. JETP **42**, 743 (1976)].

[17] L. P. Kadanoff, Ann. Phys. (NY) **100**, 359 (1976).

[18] A. N. Berker and S. Ostlund, J. Phys. C **12**, 4961 (1979).

[19] R. B. Griffiths and M. Kaufman, Phys. Rev. B **26**, 5022 (1982).

[20] M. Kaufman and R. B. Griffiths, Phys. Rev. B **30**, 244 (1984).

[21] S. R. McKay and A. N. Berker, Phys. Rev. B **29**, 1315 (1984).

[22] M. Hinczewski and A. N. Berker, Phys. Rev. E **73**, 066126 (2006).

[23] P. N. Timonin, Low Temp. Phys. **40**, 36 (2014).

[24] B. Derrida and G. Giacomin, J. Stat. Phys. **154**, 286 (2014).

[25] M. F. Thorpe and R. B. Stinchcombe, Philos. Trans. R. Soc., Ser. A **372**, 20120038 (2014).

[26] A. Efrat and M. Schwartz, Physica **414**, 137 (2014).

[27] C. Monthus and T. Garel, Phys. Rev. B **89**, 184408 (2014).

[28] T. Nogawa and T. Hasegawa, Phys. Rev. E **89**, 042803 (2014).

[29] M. L. Lyra, F. A. B. F. de Moura, I. N. de Oliveira, and M. Serva, Phys. Rev. E **89**, 052133 (2014).

[30] V. Singh and S. Boettcher, Phys. Rev. E **90**, 012117 (2014).

[31] Y.-L. Xu, X. Zhang, Z.-Q. Liu, K. Xiang-Mu, and R. Ting-Qi, Eur. Phys. J. B **87**, 132 (2014).

[32] Y. Hirose, A. Oguchi, and Y. Fukumoto, J. Phys. Soc. Jpn. **83**, 074716 (2014).

[33] V. S. T. Silva, R. F. S. Andrade, and S. R. Salinas, Phys. Rev. E **90**, 052112 (2014).

[34] Y. Hotta, Phys. Rev. E **90**, 052821 (2014).

[35] S. Boettcher, S. Falkner, and R. Portugal, Phys. Rev. A **91**, 052330 (2015).

[36] S. Boettcher and C. T. Brunson, Eur. Phys. Lett. **110**, 26005 (2015).

[37] Y. Hirose, A. Ogushi, and Y. Fukumoto, J. Phys. Soc. Jpn. **84**, 104705 (2015).

[38] S. Boettcher and L. Shanshan, J. Phys. A **48**, 415001 (2015).

[39] A. Nandy and A. Chakrabarti, Phys. Lett. A **379**, 2876 (2015).

[40] Ç. Yunus, B. Renklioğlu, M. Keskin, and A. N. Berker, Phys. Rev. E **93**, 062113 (2016).

[41] A. N. Berker, Phys. Rev. B **12**, 2752 (1975).

[42] A. N. Berker and M. Wortis, Phys. Rev. B **14**, 4946 (1976).

[43] B. Nienhuis, A. N. Berker, E. K. Riedel, and M. Schick, Phys. Rev. Lett. **43**, 737 (1979).

[44] D. Andelman and A. N. Berker, J. Phys. A **14**, L91 (1981).

[45] A. N. Berker, S. Ostlund, and F. A. Putnam, Phys. Rev. B **17**, 3650 (1978).

[46] A. N. Berker and D. R. Nelson, Phys. Rev. B **19**, 2488 (1976).

[47] J. O. Indekeu and A. N. Berker, Phys. A (Amsterdam, Neth.) **140**, 368 (1986).

[48] J. O. Indekeu, A. N. Berker, C. Chiang, and C. W. Garland, Phys. Rev. A **35**, 1371 (1987).

[49] S. R. McKay, A. N. Berker, and S. Kirkpatrick, Phys. Rev. Lett. **48**, 767 (1982).

[50] M. S. Cao and J. Machta, Phys. Rev. B **48**, 3177 (1993).

[51] A. Falicov, A. N. Berker, and S. R. McKay, Phys. Rev. B **51**, 8266 (1995).

[52] K. Hui and A. N. Berker, Phys. Rev. Lett. **62**, 2507 (1989).

[53] K. Hui and A. N. Berker, Phys. Rev. Lett. **63**, 2433 (1989).

[54] M. Hinczewski and A. N. Berker, Phys. Rev. B **78**, 064507 (2008).

[55] D. Andelman and A. N. Berker, Phys. Rev. B **29**, 2630 (1984).

[56] M. J. P. Gingras and E. S. Sørensen, Phys. Rev. B **46**, 3441 (1992).

[57] G. Migliorini and A. N. Berker, Phys. Rev. B **57**, 426 (1998).

[58] M. J. P. Gingras and E. S. Sørensen, Phys. Rev. B **57**, 10264 (1998).

[59] C. N. Kaplan and A. N. Berker, Phys. Rev. Lett. **100**, 027204 (2008).

[60] C. Güven, A. N. Berker, M. Hinczewski, and H. Nishimori, Phys. Rev. E **77**, 061110 (2008).

[61] M. Ohzeki, H. Nishimori, and A. N. Berker, Phys. Rev. E **77**, 061116 (2008).

[62] E. Ilker and A. N. Berker, Phys. Rev. E **89**, 042139 (2014).

[63] M. Demirtaş, A. Tuncer, and A. N. Berker, Phys. Rev. E **92**, 022136 (2015).

[64] P. E. Cladis, Phys. Rev. Lett. **35**, 48 (1975).

[65] F. Hardouin, A. M. Levelut, M. F. Achard, and G. Sigaud, J. Chem. Phys. **80**, 53 (1983).

[66] R. R. Netz and A. N. Berker, Phys. Rev. Lett. **68**, 333 (1992).

[67] S. Kumari and S. Singh, Phase Trans. **88**, 1225 (2015).

[68] H. Saleur, Nucl. Phys. B **360**, 219 (1991).

[69] J. L. Jacobsen, J. Salas, and A. D. Sokal, J. Stat. Phys. **119**, 1153 (2005).

[70] J. L. Jacobsen and H. Saleur, Nucl. Phys. B **743**, 207 (2006).

[71] Y. Ikhlef, Mod. Phys. Lett. **25**, 291 (2011).

[72] J. L. Jacobsen and C. R. Scullard, J. Phys. A **45**, 494003 (2012).

[73] J. L. Jacobsen and J. Salas, Nucl. Phys. B **875**, 678 (2013).

[74] C. R. Scullard and J. L. Jacobsen, J. Phys. A **49**, 125003 (2016).

[75] R. Bondesan, S. Caracciolo, and A. Sportiello, J. Phys. A: Math. Theor. **50**, 074003 (2017).

[76] J. L. Jacobsen, J. Salas, and C. R. Scullard, arXiv:1702.02006 [cond-mat.stat-mech].

[77] S. R. McKay, A. N. Berker, and S. Kirkpatrick, J. Appl. Phys. **53**, 7974 (1982).

[78] A. N. Berker and S. R. McKay, J. Stat. Phys. **36**, 787 (1984).

[79] A. J. Bray and M. A. Moore, Phys. Rev. Lett. **58**, 57 (1987).

[80] E. J. Hartford and S. R. McKay, J. Appl. Phys. **70**, 6068 (1991).

[81] M. Nifle and H. J. Hilhorst, Phys. Rev. Lett. **68**, 2992 (1992).

[82] M. Nifle and H. J. Hilhorst, Phys. A (Amsterdam, Neth.) **194**, 462 (1993).

[83] M. Cieplak, M. S. Li, and J. R. Banavar, Phys. Rev. B **47**, 5022 (1993).

[84] F. Krzakala, Europhys. Lett. **66**, 847 (2004).

[85] F. Krzakala and J. P. Bouchaud, Europhys. Lett. **72**, 472 (2005).

[86] M. Sasaki, K. Hukushima, H. Yoshino, and H. Takayama, Phys. Rev. Lett. **95**, 267203 (2005).

[87] J. Lukic, E. Marinari, O. C. Martin, and S. Sabatini, J. Stat. Mech.: Theory Exp. (2006) L10001.

[88] P. Le Doussal, Phys. Rev. Lett. **96**, 235702 (2006).

[89] T. Rizzo and H. Yoshino, Phys. Rev. B **73**, 064416 (2006).

[90] H. G. Katzgraber and F. Krzakala, Phys. Rev. Lett. **98**, 017201 (2007).

[91] H. Yoshino and T. Rizzo, Phys. Rev. B **77**, 104429 (2008).

[92] J. H. Pixley and A. P. Young, Phys Rev B **78**, 014419 (2008).

[93] T. Aspelmeier, Phys. Rev. Lett. **100**, 117205 (2008).

[94] T. Aspelmeier, J. Phys. A **41**, 205005 (2008).

[95] T. Mora and L. Zdeborova, J. Stat. Phys. **131**, 1121 (2008).

[96] N. Aral and A. N. Berker, Phys. Rev. B **79**, 014434 (2009).

[97] Q. H. Chen, Phys. Rev. B **80**, 144420 (2009).

[98] T. Jörg and F. Krzakala, J. Stat. Mech.: Theory Exp. (2012) L01001.

[99] W. de Lima, G. Camelo-Neto, and S. Coutinho, Phys. Lett. A **377**, 2851 (2013).

[100] W. Wang, J. Machta, and H. G. Katzgraber, Phys. Rev. B **92**, 094410 (2015).

[101] V. Martin-Mayor and I. Hen, Sci. Rep. **5**, 15324 (2015).

[102] Z. Zhu, A. J. Ochoa, S. Schnabel, F. Hamze, and H. G. Katzgraber, Phys. Rev. A **93**, 012317 (2016).

[103] W. Wang, J. Machta, and H. G. Katzgraber, Phys. Rev. B **93**, 224414 (2016).

[104] J. Marshall, V. Martin-Mayor, and I. Hen, Phys. Rev. A **94**, 012320 (2016).

[105] L. A. Fernandez, E. Marinari, V. Martin-Mayor, G. Parisi, and D. Yllanes, J. Stat. Mech.: Theory Exp. (2016) 123301.

[106] P. Collet and J.-P. Eckmann, *Iterated Maps on the Interval as Dynamical Systems* (Birkhäuser, Boston, 1980).

[107] R. C. Hilborn, *Chaos and Nonlinear Dynamics*, 2nd ed. (Oxford University Press, New York, 2003).